MSUHEP-150202

Sign Structure of Susceptibilities of Conserved Charges in the $(2+1)$ Polyakov Quark Meson Model

Sandeep Chatterjee*
Theoretical Physics Division, Variable Energy Cyclotron Centre, Kolkata 700064, India

Kirtimaan A. Mohan†
Department of Physics and Astronomy, Michigan State University, East Lansing, Michigan 48824, USA

arXiv:1502.00648v1 [nucl-th] 2 Feb 2015

Abstract

The sign structure of correlations of conserved charges are investigated in a QCD like model: the $(2+1)$ flavor Polyakov Quark Meson model. We compute all susceptibilities of the conserved charges on the $(\mu_B - T)$ plane up to fourth order and a few at higher order as well. By varying the mass of the sigma meson, we are able to study and compare scenarios with as well as without a critical point. In the hadron-quark transition regime we identify certain correlations that turn negative unlike expectation from ideal hadron resonance gas calculations. The striking feature being that these remain negative deep into the hadronic side and thus could be measured in experiments. Measurement of such quantities in heavy ion collision experiments can elucidate the location of the QCD transition curve and possibly the critical point.

PACS numbers: 12.38Mh, 25.75.Nq, 12.38.Gc

---

* sandeepc@vecc.gov.in
† kamohan@pa.msu.edu

The phase diagram of Quantum Chromodynamics (QCD), the theory of strongly interacting matter, has been a subject of intense study both theoretically and experimentally for some time now. The thermodynamic state of the strongly interacting medium which is expected to be created in a heavy ion collision (HIC) experiment can be specified by four quantities: temperature T and three chemical potentials corresponding to the conserved charges baryon number B, electric charge Q and strangeness S, namely μ_B, μ_Q and μ_S respectively. The QCD degrees of freedom are sensitive to these thermodynamic quantities resulting in a rich phase diagram [1, 2]. At zero chemical potentials ($\mu_B = \mu_Q = \mu_S = 0$), first principle Lattice QCD (LQCD) Monte-Carlo simulations have shown that QCD undergoes a smooth analytic crossover transition from the low T hadron resonance gas (HRG) phase to the high T phase of quarks and gluons (QGP) [3, 4]. At non zero but small μ_B/T, recent LQCD results [5, 6] show similar behavior.

However, the QCD phase diagram for $\mu_B/T \gtrsim 1$ is far from established. Direct first principle techniques of LQCD using Monte-Carlo methods fail due to the sign problem [7, 8]. This is where QCD like models which have been tuned to reproduce LQCD results at zero μ_B could provide valuable insight about the nature of the QCD medium [9–18]. Model computations at large μ_B/T predict the possibility of a first order phase transition [9–18]. Thus the location of the critical point (CP) which is the end point of this first order transition line where there is a second order phase transition is an important landmark on the QCD phase diagram. Mapping the phase transition line and the CP is a major goal of the heavy ion collision experiments [19].

The CP dynamics gives rise to diverging correlation length that result in non-monotonic variations of some quantities which have been proposed as plausible observables to identify the CP [20]. For example, moments of conserved charges that can be extracted experimentally through event by event analyses are good candidates to hunt for the CP [21, 22]. At zero μ_B, with three flavors of quarks there are numerous computations of the susceptibilities both on the lattice [23–26] as well as in models [27–33]. Recently, for non-zero but small μ_B/T, susceptibilities have been computed on the lattice [34–36]. Some of these cumulants have also been computed on the $\mu_B - T$ plane in models [29, 37].

Such observables are good markers of the CP, as long as they are measured close to the CP, the location of which is unknown. Further, in HIC experiments, the produced fireball has finite size and lifetime which can tame the divergence of the correlation length and render it finite. This will blur the effects of singularity in the critical region and hence diminish the chances of a direct experimental confirmation of the CP [38–40]. Thus, rather than looking at the absolute values of the susceptibilities, sign structures of the same might be better suited for such studies [40]. Third moments of conserved charges like B, Q and energy have been already studied in this regard [40]. These were found to change sign at the hadron-quark phase boundary corresponding to peak like structures of second order susceptibilities. Studies based on the Polyakov Quark Meson (PQM) model show that higher order cumulants of B and Q become negative valued in the transition regime [41, 42]. It has been suggested that such distinctive sign structures follow from the scaling functions of the 3-D $O(4)$ universality class [42]. Higher order generalized susceptibilities for B and their sign structure in the phase diagram was studied in the $(2 + 1)$ PQM model [37]. For all the above cases, the negative regions were found very close to the phase boundary and mostly on the QGP side. It is interesting to note that LQCD computations along the chemical freeze-out curve as determined from HRG analysis of yields show that the kurtosis of B exhibits a change of sign around $\sqrt{S_{NN}} \sim 20$ GeV [43]. This has been attributed to proximity to the CP [43]. Such sign structures of susceptibilities due to the quark-hadron transition regime and the CP can be observed if the chemical freeze-out (CFO) curve also passes very close to the phase boundary or the dynamics is such that the sign structures are retained during expansion between the phase boundary and the CFO curve. However, observation of negative baryonic kurtosis has remained elusive so far in the Beam Energy Scan (BES) program at RHIC [44]. This motivates us to investigate the sign structures of the off-diagonal components of the correlations of conserved charges which has so far been ignored. In this paper we work with the $(2 + 1)$ flavor PQM model at the mean field level and analyze the sign structures of the cumulants of conserved charges on the $(\mu_B - T)$ plane with and without CP. We do not find any unique sign structure that could be attributed to the presence of the CP alone. On the other hand, there are a few candidates, as summarized in Table II, that are sensitive to the crossover/transition region whether or not there is a CP and show a change of sign. Thus these observables are good indicators of the transition regime. Some of these off-diagonal susceptibilities were found to exhibit negative regions that extend deep into the hadronic side and hence could be more easily accessible to experiments.

The rest of this paper is organized as follows: In Section I, we provide the details of the PQM model and its parameters used in this study. We further define the susceptibilities that are studied here and their connections with the corresponding moments of the conserved charges that are experimentally measurable. In Section II, we first compare our model computations with those of lattice at non-zero but small μ_B/T. We compare, with lattice, some cumulants as well as the values of the strangeness chemical potential obtained by imposing the strangeness neutrality condition. We then present our results on various cumulants on the $\mu_B - T$ plane and comment on their usefulness in mapping out the QCD phase diagram, namely identifying the transition regime and the location of the CP. Finally, in Section III, we summarize and conclude.

I. FORMALISM

The relevant thermodynamic potential $\Omega\left(T, \mu_B, \mu_Q, \mu_S\right)$ in the $(2+1)$ flavor PQM with the inclusion of the vacuum term at a temperature T and chemical potentials μ_B, μ_Q and μ_S in the mean field approximation is given in Refs. [45, 46]. The pressure Pr is given by

$$Pr\left(T, \mu_B, \mu_Q, \mu_S\right) = -\Omega\left(T, \mu_B, \mu_Q, \mu_S\right) \ . \tag{1}$$

The cumulants of the conserved charges are computed by taking appropriate derivatives of Pr

$$\chi_{ijk}^{BQS}\left(T, \mu_B, \mu_Q, \mu_S\right) = \frac{\partial^{i+j+k}(Pr/T^4)}{\partial\left(\mu_B/T\right)^i \partial\left(\mu_Q/T\right)^j \partial\left(\mu_S/T\right)^k} \ . \tag{2}$$

These generalized susceptibilities are related to the moments of the distribution of the conserved charges such as the mean M, variance σ^2, skewness S etc. The derivatives in eq. (2) have been computed numerically using the package `ADOL-C` [47, 48] which allows efficient computation of higher order susceptibilities without further truncation errors.

When relating to heavy ion collision experiments, there are two constraints to be met. Since the number of participating nucleons is not fixed a priori, the net baryon number N_B or electric charge N_Q can not be fixed independently. But, the ratio of N_B to N_Q can be fixed to that of the initial heavy ion used in the experiment (~ 2.5). Since the incoming heavy ions carry zero net strangeness N_S, the condition of vanishing N_S also has to be imposed.

$$N_B/N_Q = 2.5 \tag{3}$$

$$N_S = 0 \tag{4}$$

Eqs. (3) and (4) fix μ_Q and μ_S respectively. In this work we will mainly present our results for 3 different variants of the $(2+1)$ flavor PQM model: msig400, msig400-phys and msig600. These differ from each other on the choice of the mass of the sigma meson m_σ and also the way we treat μ_S and μ_Q. We have used $m_\sigma = 400$ MeV for msig400 and msig400-phys while for msig600 we put $m_\sigma = 600$ MeV. While msig400 and msig400-phys possess a CP on the $(\mu_B - T)$ plane, msig600 has no CP on the phase diagram [45]. Thus we are able to study and compare the effects of the CP on the sign structures. In order to understand the effects of non-zero μ_S and μ_Q, for msig400 and msig600 we use $\mu_S = 0$ and $\mu_Q = 0$ while for msig400-phys we use μ_S and μ_Q as obtained from eqs. (3) and (4). In Table I, we have listed the above scenarios with their descriptions for easy reference

	msig400	msig400-phys	msig600
m_σ (MeV)	400	400	600
μ_S	0	from (3) and (4)	0
μ_Q	0	from (3) and (4)	0
CP	yes	yes	no

TABLE I. The distinct features of the different variants of the PQM model investigated here.

II. RESULTS

In our earlier works [45, 46], we had shown good qualitative agreements between LQCD data and PQM model predictions at zero chemical potential for a large number of thermodynamic quantities like pressure, entropy density, energy density, specific heat, speed of sound etc., and also for some susceptibilities of conserved charges up to sixth order. LQCD data are now available also at non-zero but small μ_B/T and also for non-zero μ_S and μ_Q satisfying Eqs. (3) and (4) [35, 36]. Before we present our model results for the susceptibilities on the entire $\mu_B - T$ plane, we perform a comparative study between LQCD and our model at small μ_B/T. Here we will particularly look at the extracted values of μ_S and few ratios of susceptibilities at non-zero μ_B/T.

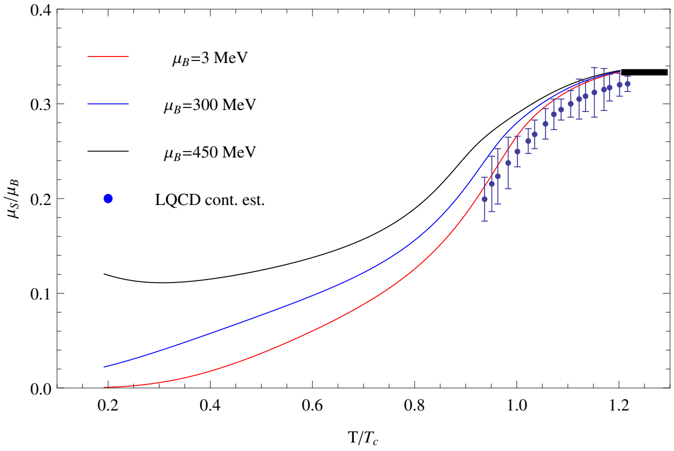

FIG. 1. Ratio of μ_S/μ_B with T/T_c for different values of μ_B obtained in model and compared to leading order results obtained in LQCD [49]. The thick black line denotes the SB limit.

A. μ_S/μ_B: Model vs Lattice

For a realistic estimate of thermodynamic observables related to the QGP experiments, it is important that the computations are done for non-zero μ_S and μ_Q obtained from the conditions as imposed by eqs. (3) and (4). We have implemented this and extracted the values of μ_S and μ_Q for different T and μ_B. In Fig. 1 we show μ_S normalized to μ_B for several values of $\mu_B = \{3, 300, 450\}$ MeV. We have compared these model values with the continuum estimates obtained in LQCD [49] and find good agreement. μ_S/μ_B seems to have a monotonically increasing behavior with T/T_c, with a faster rise around T_c and finally saturates in the QGP phase to $\sim 1/3$ (shown by the thick black line in Fig. (1)). This limiting value can be understood easily in the context of a Stefan-Boltzmann (SB) gas of ideal quarks and gluons. In the SB limit, only the strange quarks which carry both S and B decide the μ_S/μ_B value. Now in order to ensure that Eq. (3) is obeyed, the fugacity factors for strange and anti-strange quarks should be unity. Since strange quarks carry $B = 1/3$ and $S = -1$ while anti-strange quarks carry $B = -1/3$ and $S = 1$, it turns out that in order to ensure $B\mu_B + S\mu_S = 0$, μ_S/μ_B must be $-B/S = 1/3$. We have ignored μ_Q in this discussion since its value is much less than both μ_S and μ_B. Thus the SB limit is independent of μ_B and we see this also in the Fig. 1 where different μ_B curves all saturate to 1/3 in the QGP side. On the contrary, in the low T regime where the degrees of freedom are hadronic, μ_S/μ_B is much more sensitive to μ_B. This is because in the hadronic regime unlike the ideal quark gluon gas, strangeness carriers can be both: baryonic (eg.Λ) and non-baryonic or mesonic (eg. kaons). If we had a mesonic gas, $\mu_S = 0$ will always be the solution of Eq. 3. Non-zero values of μ_S arise only because of the strange baryons. Since there is a large mass difference of the order of 700 MeV between the lightest strange meson and baryon, depending on T the relative contribution of the strange baryons differ from that of the strange mesons, rising monotonically with T. This results in the monotonically increasing behavior of μ_S/μ_B with T/T_c for constant μ_B. Again, with increasing value of μ_B the strange baryon contribution increases and this results in a larger value of μ_S/μ_B for same T.

B. $\frac{\chi_1^Q}{\chi_2^Q}, \frac{\chi_1^B}{\chi_2^B}$: Model vs Lattice

Recently, a lot of effort has been invested in computing susceptibilities at non-zero μ_B in LQCD in order to confront them with experimentally measured moments of B, Q and S [34–36]. Such a comparison will enable a determination of the CFO T and μ_B, bridging the gap between LQCD and experiments. This is a complementary program to the already quite successful endeavor of determining the freeze-out conditions by comparing the hadron yields between experiments and hadron resonance gas models [50–53]. In Refs. [35, 36], the (μ_B/T) variation of the ratio $R_{12}^X = \chi_1^X/\chi_2^X$ for $X = B$, Q have been measured on the lattice. A comparison between theory and experiment of these ratios can provide an estimate of μ_B at CFO [35]. In Fig. 2 we have plotted these quantities as obtained in PQM and compared

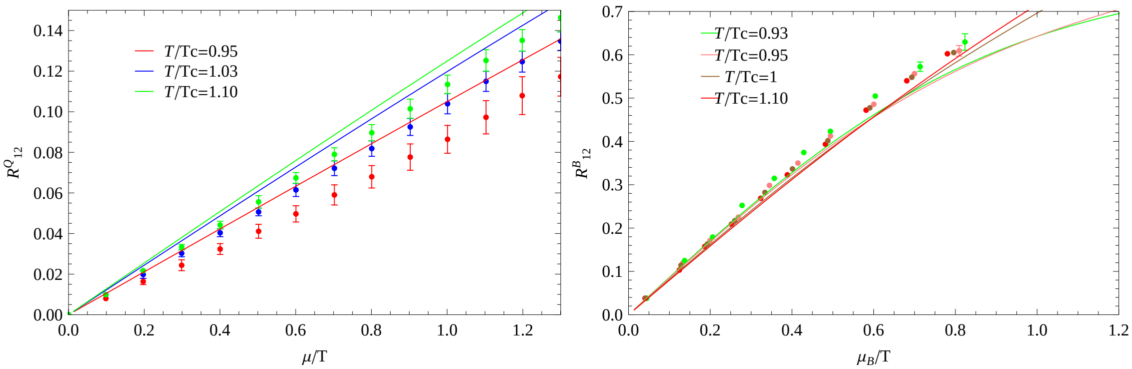

FIG. 2. Ratios of susceptibilities: $R^Q_{12} = \chi^Q_1/\chi^Q_2$ compared with HotQCD [35] and $R^B_{12} = \chi^B_1/\chi^B_2$ compared with WB [36] lattice data.

them with the HotQCD lattice data [35] as well as WB lattice data [36]. Both lattice as well as PQM show an almost linear variation of R^Q_{12} with μ_B/T in the range $0 < \mu_B/T < 1$. The model over predicts the lattice data in the entire range. For example, at $\mu_B/T \sim 1$, the model is about 20% more than the lattice. We should note that there is an uncertainty in the determination of T_c adjusting which it is possible to get a better agreement between model and lattice. However, here our main intention in performing this comparison is to demonstrate the good qualitative agreement between LQCD and PQM model predictions. This gives us faith to trust the PQM results on the $\mu_B - T$ plane where there is yet to be any lattice data. Thus, having set the platform for a discussion of the PQM results at non-zero μ_B, we go into the next section where we report on the novel qualitative features of the sign structures of the generalized susceptibilities whose measurements in heavy ion collision experiments could shed light on the features of the QCD phase diagram.

C. Sign Structures of Susceptibilities: Model

Having found good qualitative agreement between PQM and LQCD at non-zero μ_B, we will now analyze the sign structures of various fluctuations and correlations of conserved charges on the $(\mu_B - T)$ plane. We shall focus mainly on the transition regime between the HRG and QGP phases. The transition region can be broadly classified into three categories: firstly for small μ_B/T there is a smooth crossover and no true phase transition. Secondly, for large enough μ_B/T, we expect a first order phase transition. Thirdly, in the intermediate range of μ_B/T, one thus expects a critical region with a second order phase transition at the CP where the line of first order phase transition meets the crossover line. The existence and location of this CP is a topic of intense current research. In PQM, the location of the CP is highly sensitive to the value of m_σ used. For example, with $m_\sigma \geq 600$ MeV one finds no CP [45]. In order to understand the distinguishing features of the QCD phase diagram with and without a CP and also the effect of non-zero μ_Q and μ_S, we have computed the susceptibilities for three different variants of PQM as outlined in Table I: msig400, msig400-phys and msig600. We will now report our findings on the sign structure of several susceptibilities up to sixth order in these different regions of the QCD phase diagram for the three cases.

Before we proceed, please note that all figures shown henceforth will be plots on the $\mu_B - T$ plane. In fact, since we are interested only in the qualitative features of negative correlations, we scale the T axis (x-axis) by T_c (the cross-over temperature at $\mu_B = 0$) and the μ_B axis (y-axis) by μ_c (the μ_B value where the first order phase transition line meets the μ_B axis). In all plots we show the smooth cross-over curve in blue dashed lines. The CP is denoted by a red dot whereas a black (thick) solid line denotes the first order phase transition line. Contours of various susceptibilities are shown with boxed numbers indicating the numerical value of the susceptibilities along those contours. Finally, regions of negative correlation are indicated by orange (shaded) regions.

1. *Diagonal Susceptibilities up to 4th order*

We have shown the baryonic susceptibilities up to 4th order in Figure. 3. Experimentally only net proton number is obtained as the neutrons are never observed. Cumulants of net proton number act as proxy to the susceptibilities of the net baryon number. Up to 2nd order there are no zero contours and therefore no regions of negative correlation. The first appearance of a negative region is for χ_3^B. It spans through the crossover as well as first order phase transition regions. For all the three cases studied here, the negative region is located just above the hadron-quark transition on the QGP side. For χ_4^B, the negative region is only in the crossover region and terminates at the CP. Negative values for χ_4^B/χ_2^B have also been measured on lattice at non-zero μ_B [43]. For the case of msig600, even though the CP is absent, there is a negative region in the transition regime that stretches all the way up to very small T. Thus, we see that negative regions in χ_3^B and χ_4^B only imply the proximity of the hadron-quark transition region that may or may not include a CP. Thus negative values of χ_3^B and χ_4^B do not necessarily imply the existence of a CP. We have not shown plots of the susceptibilities of Q as the sign structure for the electric charge susceptibilities look similar to that of the baryonic ones. The contours of S susceptibilities on the $(\mu_B - T)$ plane are devoid of any interesting sign structures. The χ_2^S susceptibilities are shown in Fig. 4. We note that in msig400-phys where the physical conditions of eqs. (3) and (4) are imposed, the diagonal strange susceptibilities are affected strongly and are distinctly different from what one obtains in msig400 and msig600. In msig400-phys the variation of χ_2^S along μ_B becomes gentler with the contours being almost parallel to the μ_B axis.

2. *Mixed susceptibilities of order two*

Neither χ_{11}^{BQ} nor $-\chi_{11}^{BS}$ have any interesting sign structure. Neither have any negative regions. On the other hand, χ_{11}^{QS} has a narrow region where it turns negative for msig400 and msig600. Interestingly, this region of negative susceptibilities lies in the hadronic side. Fig. 5 shows χ_{11}^{QS} which has negative values for large μ_B close to the transition region and within the hadronic phase. For msig400 we see that the region is close to the CP. For msig400-phys we observe that regions of negative correlation are in fact reduced and very close to the CP. Since negative correlations are also seen for msig600, we infer that a measurement of negative values of this correlation does not necessarily confirm a CP.

3. *Mixed susceptibilities of order three*

The third order mixed susceptibilities show more interesting behavior. In Fig.6, we show χ_{12}^{QS} and χ_{111}^{BQS}. For msig400-phys, there is a large region deep into the HRG phase where χ_{12}^{QS} is negative. Thus, there is a possibility that the CFO curve passes through this region and these negative regions could be observed in experiments. Interestingly, for both msig400 and msig600 where μ_Q and μ_S are zero this negative region is highly localized on the first order line. χ_{12}^{BS} which is not shown here has small negative valued region along the crossover line from the CP in msig400. However, this effect is absent in msig400-phys and msig600 and therefore probably cannot be used to probe the CP in experiment. For χ_{111}^{BQS}, all the variants show negative region in the hadronic side, though they do not extend as deep as in the case of χ_{12}^{QS}. Interestingly, the region of negative correlation extends deeper into the hadronic region for msig400-phys For the remaining off diagonal susceptibilities of order 3 we find that none of them have regions of negative correlation in the hadronic phase, although some of them have negative regions in the QGP phase close to the transition curve.

4. *Mixed susceptibilities of higher order*

In Fig. 7 we show only those fourth order off-diagonal susceptibilities that have regions of negative correlation that penetrate the hadronic phase significantly. χ_{112}^{BQS} and χ_{13}^{QS} have negative values only in the hadronic phase [1]. We observe that while χ_{112}^{BQS} extends deep into the hadronic phase, χ_{13}^{QS} is highly localized near the transition region and the CP. Also while the negative region for χ_{112}^{BQS} appears extended in msig400-phys as compared to the other cases, the opposite effect is observed in χ_{13}^{QS} where the negative region diminishes slightly. For χ_{211}^{BQS} and χ_{31}^{QS} regions of negative correlation exist on either side of the QCD transition line at large μ_B and close to the CP. These regions

---

[1] Other negative regions seen in the plot are deep in the QGP phase and we disregard them.

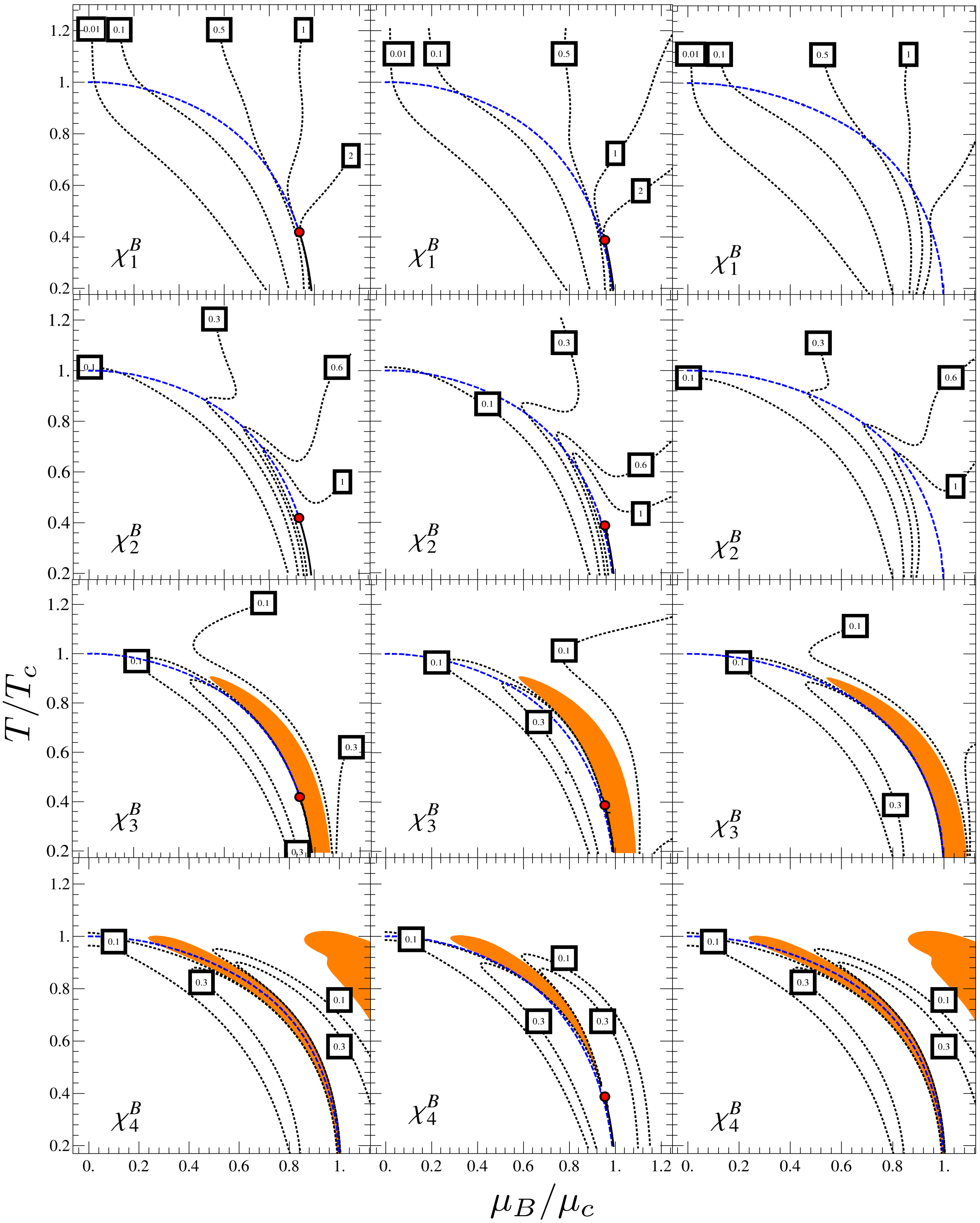

FIG. 3. Contours (black dotted) for diagonal susceptibilities up to fourth order, shown on the $\mu_B - T$ plane. Also shown are the cross-over curve (blue dashed) the CP (red dot) and the first order transition curve (black solid). Boxed number indicate the value of the susceptibilities along that contour. Negative regions are shown in orange (shaded). The three columns are for the three different variants of the PQM model in Table I. Column 1: msig400 , Column 2 : msig400-phys and Column 3: msig600

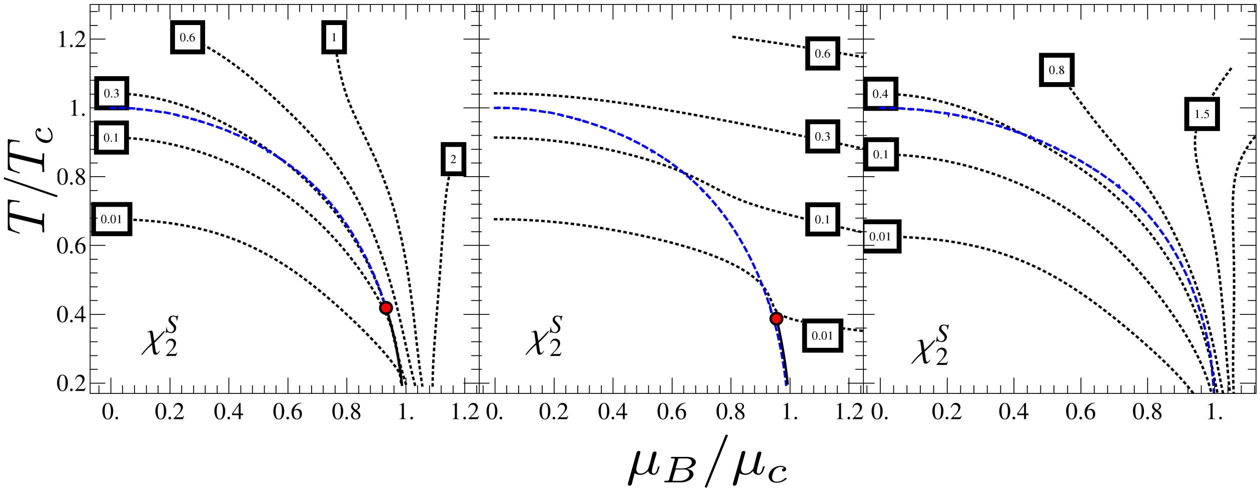

FIG. 4. Contours (black dotted) for χ_2^S shown on the $\mu_B - T$ plane. Also shown are the cross-over curve (blue dashed) the CP (red dot) and the first order transition curve (black solid). Boxed number indicate the value of the susceptibilities along that contour. Negative regions are shown in orange (shaded). The three columns are for the three different variants of the PQM model in Table I. Column 1: msig400 , Column 2 : msig400-phys and Column 3: msig600

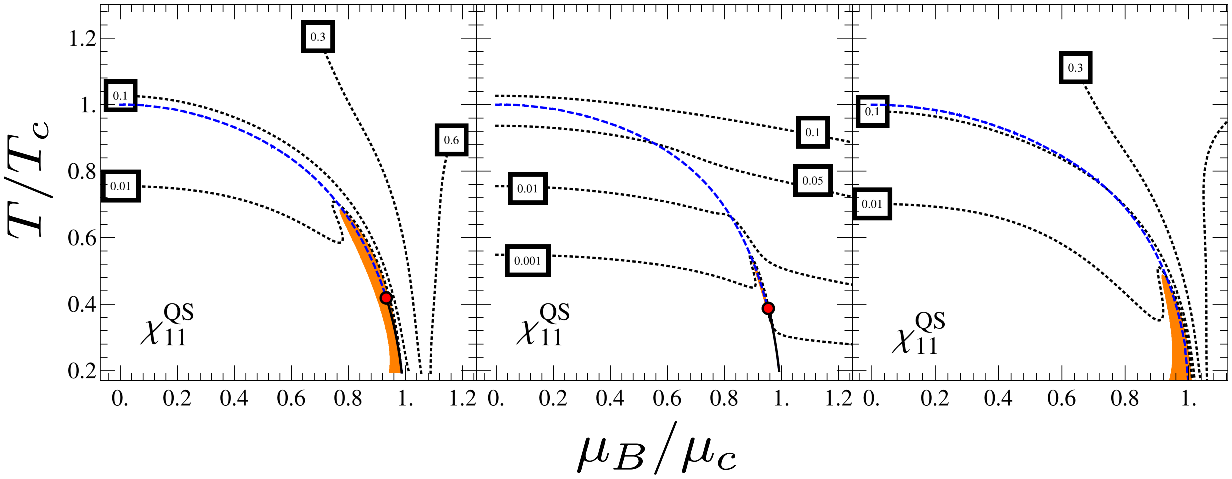

FIG. 5. Contours (black dotted) for χ_{11}^{QS}, shown on the $\mu_B - T$ plane. Also shown are the cross-over curve (blue dashed) the CP (red dot) and the first order transition curve (black solid). Boxed number indicate the value of the susceptibilities along that contour. Negative regions are shown in orange (shaded). The three columns are for the three different variants of the PQM model in Table I. Column 1: msig400 , Column 2 : msig400-phys and Column 3: msig600

appear as two separate lobes that merge across the first order transition curve and separate above the CP where the nature of the transition is that of a cross-over. χ_{211}^{BQS} shows a slightly enhanced region of negative correlation for the physical conditions of msig400-phys in comparison to the other cases while the negative regions are reduced for χ_{31}^{QS} in msig400-phys. In Fig.8 we show the contours for χ_{222}^{BQS} which has a behavior similar to the diagonal susceptibilities, with the region of negative correlation closely following the QCD transition curve and proceed into the QGP side.

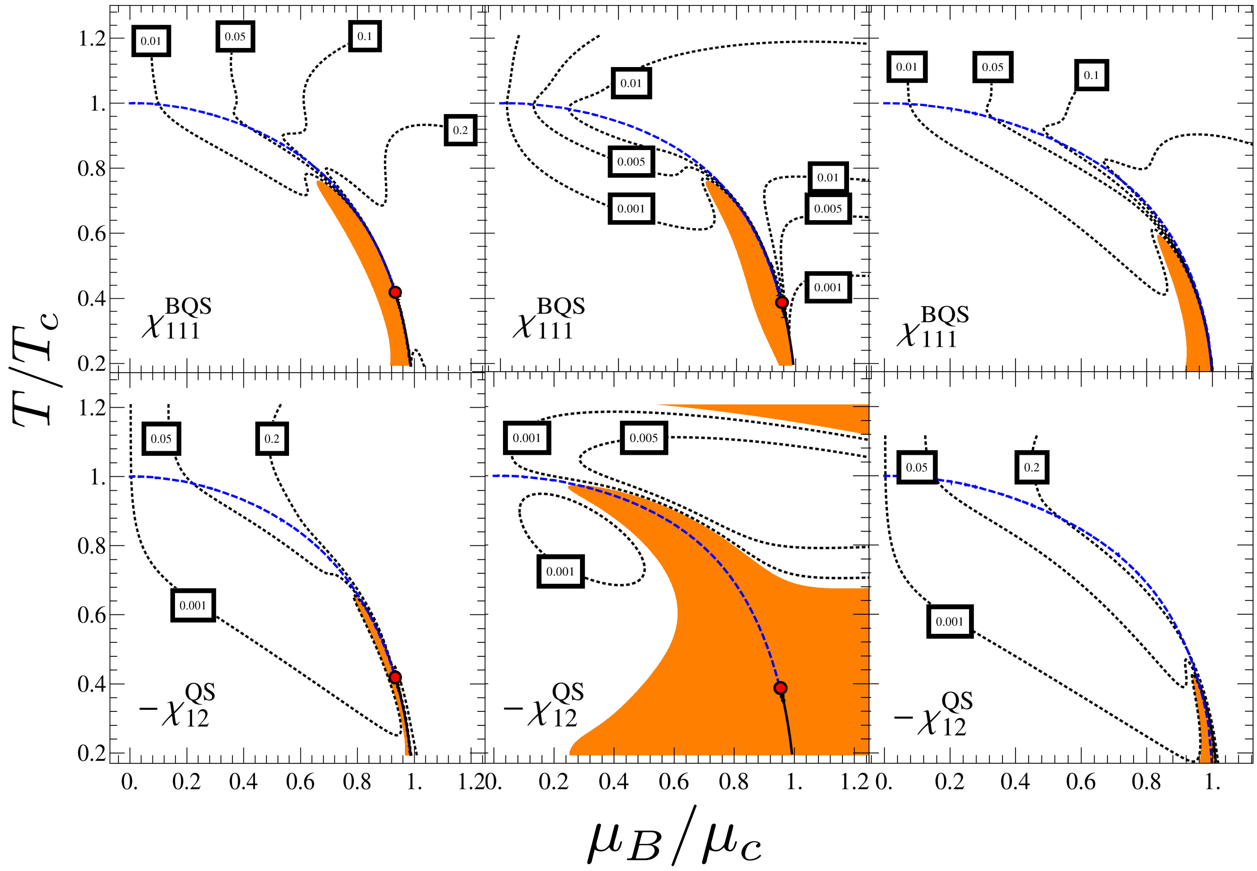

FIG. 6. Contours (black dotted) for χ_{111}^{BQS} and $-\chi_{12}^{QS}$, shown on the $\mu_B - T$ plane. Also shown are the cross-over curve (blue dashed) the CP (red dot) and the first order transition curve (black solid). Boxed number indicate the value of the susceptibilities along that contour. Negative regions are shown in orange (shaded). The three columns are for the three different variants of the PQM model in Table I. Column 1: msig400 , Column 2 : msig400-phys and Column 3: msig600

D. Tracking the QCD phase transition

After a brief description of the essential features of the sign structure of various susceptibilities in the discussion above, we would like to indicate how a measurement of the same might be useful in locating the QCD phase transition curve as well as the CP. In Fig. 9, we show along with the phase transition curve, negative regions of a few select susceptibilities, namely χ_4^B, χ_{111}^{BQS}, $-\chi_{12}^{QS}$, χ_{112}^{BQS}, χ_{211}^{BQS} and χ_{31}^{QS}. We include the diagonal χ_4^B susceptibility in this plot to accentuate the fact the off-diagonal susceptibilities have regions of negative correlation significantly deeper in the hadronic phase. It is our proposal that a systematic measurement of these off-diagonal susceptibilities can provide valuable information about the proximity of the phase transition curve as well as the CP.

In order to illustrate this point, let us consider a hypothetical CFO curve as indicated by the (gray dashed line). The curve has been drawn by scaling the phase transition curve down by a factor $R = 0.93$ and hence our CFO curve follows the phase transition curve. We have marked four points (labeled: A, B, C, and D) at various values of (μ_B, T) along this curve that indicate possible freeze-out points at which the sign of the susceptibilities can be determined. Point A, at high T and low μ_B (akin to the experiments at LHC) would not show negative values of the susceptibilities under consideration. At lower energies and larger μ_B, we approach point B where we might obtain the negative values for one of the susceptibilities, namely $-\chi_{12}^{QS}$. As we proceed to point C along the CFO, we now have three negative susceptibilities; $-\chi_{12}^{QS}$, χ_{112}^{BQS} and χ_{111}^{BQS}. Finally at point D, in addition to these three susceptibilities, χ_{111}^{BQS} is also negative. This indicates that point D is closest to the CP.

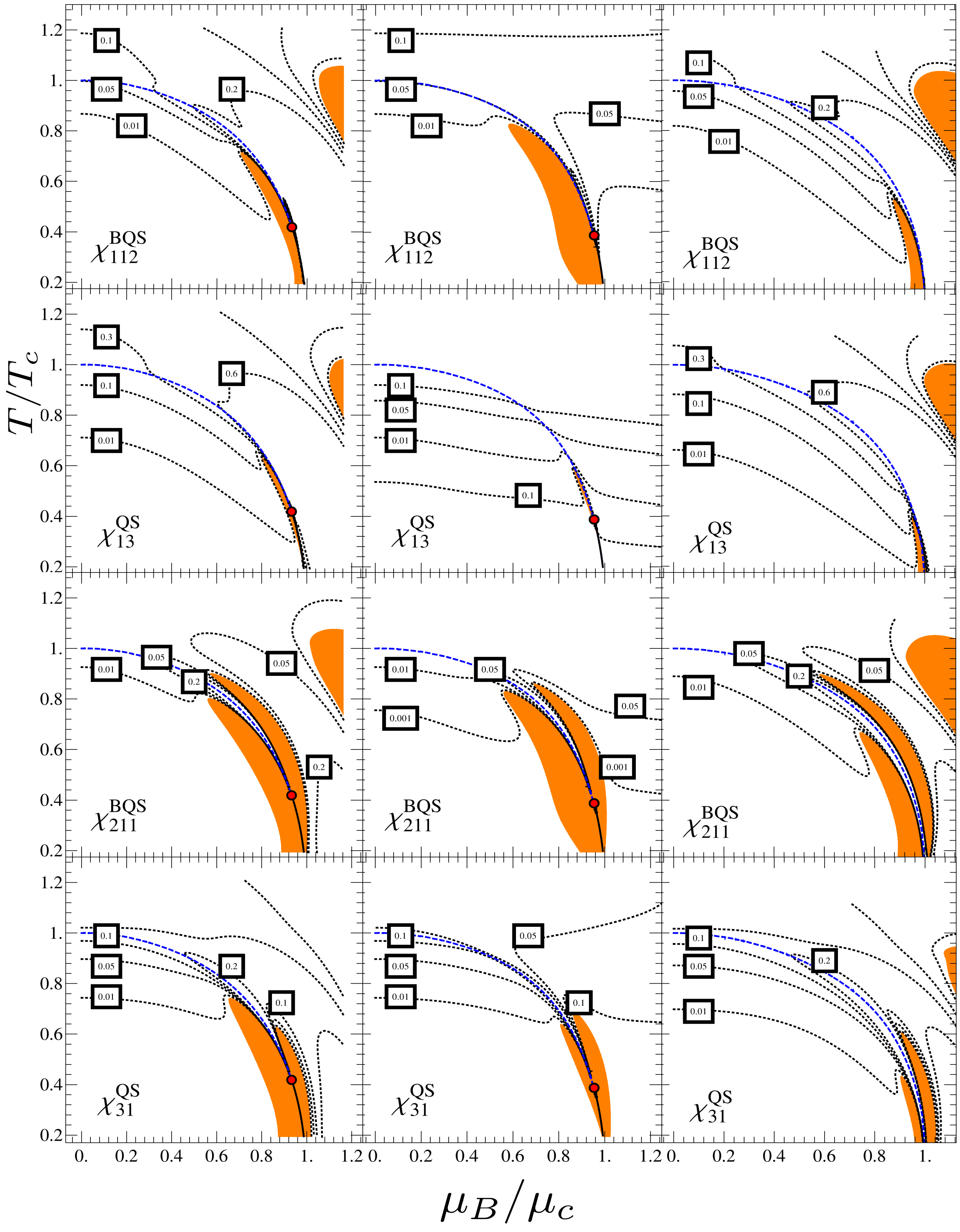

FIG. 7. Contours (black dotted) for fourth order off-diagonal susceptibilities, shown on the $\mu_B - T$ plane. Also shown are the cross-over curve (blue dashed) the CP (red dot) and the first order transition curve (black solid). Boxed number indicate the value of the susceptibilities along that contour. Negative regions are shown in orange (shaded). The three columns are for the three different variants of the PQM model in Table I. Column 1: msig400 , Column 2 : msig400-phys and Column 3: msig600

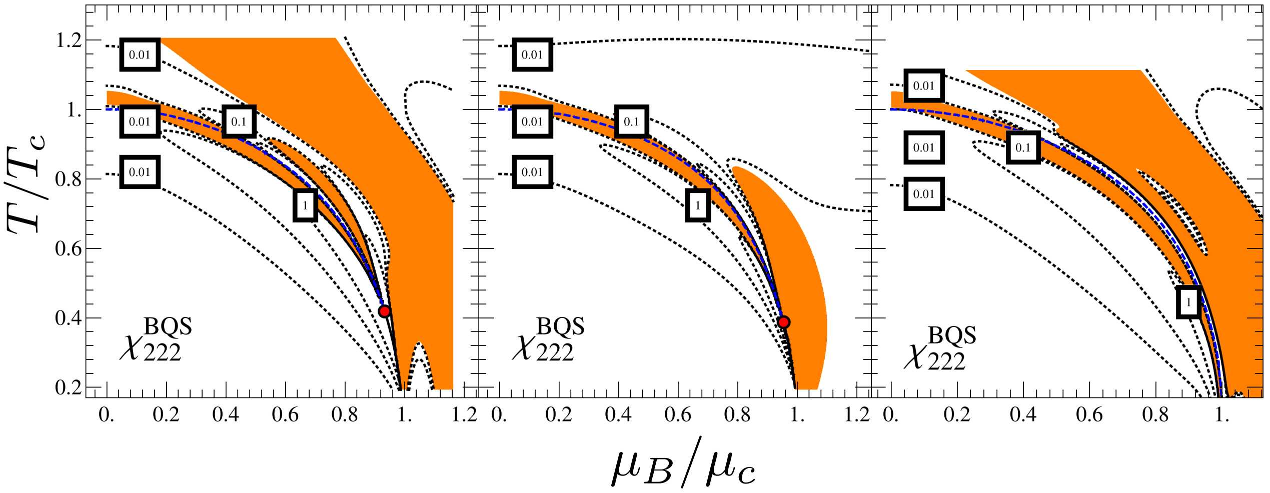

FIG. 8. Contours (black dotted) χ_{222}^{BQS}, shown on the $\mu_B - T$ plane. Also shown are the cross-over curve (blue dashed) the CP (red dot) and the first order transition curve (black solid). Boxed number indicate the value of the susceptibilities along that contour. Negative regions are shown in orange (shaded). The three columns are for the three different variants of the PQM model in Table I. Column 1: msig400 , Column 2 : msig400-phys and Column 3: msig600

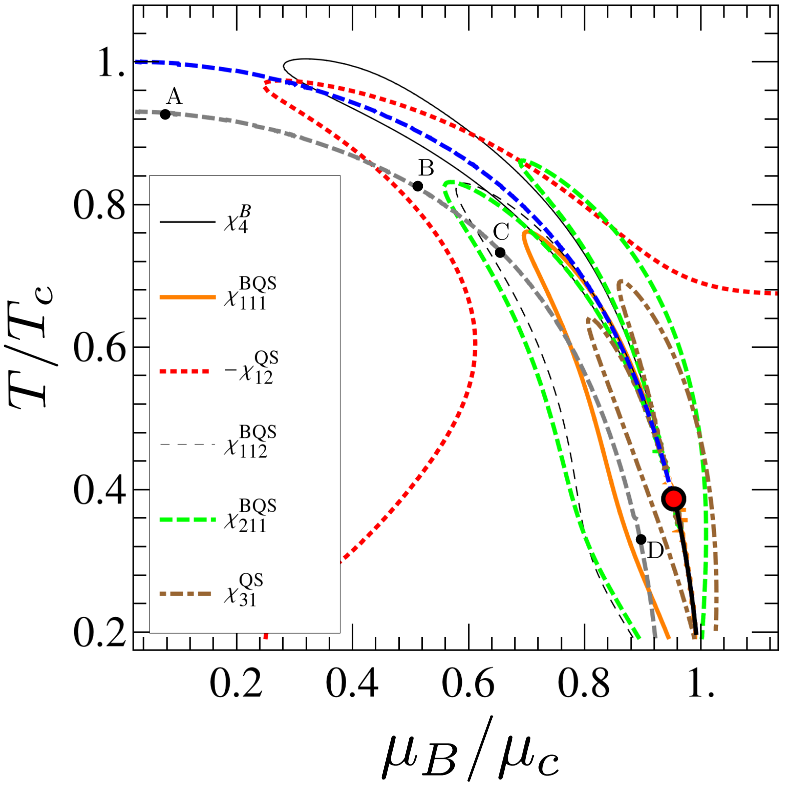

FIG. 9. Contours of negative regions for various susceptibilities for msig400-phys. The gray thick dashed curve corresponds to the proxy freeze-out line. Also shown are the cross-over curve (blue dashed) the CP (red dot) and the first order transition curve (black solid).

Susceptibility	Negative Region	Negative in Hadronic Phase	Range	R
χ_1^B	✗	–	–	–
χ_2^B	✗	–	–	–
χ_3^B	✓	✗	(0.6,0.9)-E	–
χ_4^B	✓	✓	(0.3,1.0)-CP	0.98
χ_1^Q	✗	–	–	–
χ_2^Q	✗	–	–	–
χ_3^Q	✓	✗	(0.9,0.5)-E	–
χ_4^Q	✓	✗	(0.7,0.9)-CP	–
χ_2^S	✗	–	–	–
χ_3^S	✗	–	–	–
χ_4^S	✗	–	–	–
χ_{11}^{BQ}	✗	–	–	–
χ_{11}^{BS}	✗	–	–	–
χ_{11}^{QS}	✓	✓	(0.9,0.6)-CP	0.99
χ_{111}^{BQS}	✓	✓	(0.7,0.7)-E	0.91
χ_{12}^{BQ}	✓	✗	(0.9,0.7)-E	–
χ_{21}^{BQ}	✓	✗	(0.5,0.9)-E	–
χ_{12}^{BS}	✗	–	–	–
χ_{21}^{BS}	✓	✗	(0.9,0.6)-CP	–
χ_{12}^{QS}	✓	✓		
χ_{21}^{QS}	✓	✗	(0.6,0.9)-E	–
χ_{211}^{BQS}	✓	✓	(0.6,0.8)-E	0.84
χ_{121}^{BQS}	✓	✓	(0.7,0.9)-CP	0.99
χ_{112}^{BQS}	✓	✓	(0.6,0.8)-E	0.84
χ_{22}^{BQ}	✓	✓	(0.4,0.9)-CP	0.99
χ_{22}^{BS}	✓	✗	(0.6,0.9)-E	–
χ_{22}^{QS}	✓	✗	(0.9,0.7)-E	–
χ_{31}^{BQ}	✓	✓	(0.2,0.1)-CP	0.98
χ_{13}^{BQ}	✓	✓	(0.4,1.0)-CP	0.99
χ_{31}^{QS}	✓	✓	(0.8,0.6)-E	0.96
χ_{13}^{QS}	✓	✓	(0.8,0.6)-CP	0.99
χ_{31}^{BS}	✓	✓	(0.4,1.0)-CP	0.99
χ_{13}^{BS}	✗	–	–	–
χ_{23}^{BS}	✓	✗	(0.4,0.9)-CP	–
χ_{113}^{BQS}	✓	✓	(0.8,0.7)-E	0.92
χ_{14}^{BS}	✗	–	–	–
χ_{222}^{BQS}	✓	✓	()-CP	0.96
χ_{33}^{BS}	✓	✓	(0.2,1.0)-CP	0.97
χ_{213}^{BQS}	✓	✓	(0.6,0.8)-E	0.87
χ_{123}^{BQS}	✓	✓	(0.5,0.9)-CP	0.98
χ_{24}^{BS}	✓	✓	(0.3,1)-E	0.99
χ_{114}^{BQS}	✓	✓	(0.7,0.7)-E	0.87
χ_{15}^{BS}	✗	–	–	–

TABLE II. Summary Table: A list of various susceptibilities with a description of their negative regions. The second column indicates the presence of regions of negative correlation with a tick and absence with a cross. The third column indicates whether any part of the negative region lies in the hadronic phase. The fourth column corresponds to the approximate range of the region (see text for meaning). The last column denotes the extent of the negative region into the hadronic side (see text for details). Here R corresponds to a scaling factor as described in the text.

One must be wary that the CFO curve might have a more complicated shape than the simple scaled curve that we have used. In which case the CFO curve may miss some of the negative regions. Nevertheless, measurement of negative values of the susceptibilities we have considered here are indicative of proximity to the phase transition region. Most importantly, since these susceptibilities are negative deep in the hadronic phase, the CFO curve is more likely to pass through them.

Before we conclude, we summarize our findings in Table II. In this table we list various susceptibilities and describe some of their properties. In the second column we of the table we indicate the presence of region of negative correlation by a tick mark and the absence of one by a cross. In the third column we indicate whether there there is a region of negative correlation in the hadronic phase. In the last two columns we map out regions of negative correlation. This we do by first observing that a common characteristic of negative regions is that they originate at some point of the $\mu_B - T$ plane and follow the phase transition curve. The negative regions terminate either at the CP or follow the phase transition curve all the way up to the end (E) at zero T. The fourth column thus indicates the point at which the negative region begins ($\mu_B/\mu_c, T/T_c$) and whether it follows the phase transition curve up to the CP or to the end (E). Finally, for those susceptibilities that have negative regions in the hadronic phase we give the least value of the scale factor (R) for which our hypothetical CFO curve (described above) just touches the negative region. As can be gleaned from the table, there are several useful candidates that could be used to locate the QCD phase transition curve and CP.

III. CONCLUSION

The sign structure of diagonal susceptibilities have been studied previously with negative regions found in the HRG-QGP transition regime and mostly in the QGP side. Thus only if CFO occurs close to the phase transition regime are these negative regions likely to be observed. HRG analysis of yields reveal that the CFO curve is close to the QCD transition curve for small μ_B as in the case of LHC [50–53]. At SPS and future experiments like FAIR where μ_B is large, the CFO curve could be further away from the transition curve and therefore it is likely that these experiments may miss the negative regions. In this study we find that for particular choices of off-diagonal susceptibilities as listed in Table II, negative regions could extend deep into the hadronic phase and should be accessible to the experiments even at large values of μ_B. Our study suggest that the correlations of conserved charges exhibit a rich sign structure in the $\mu_B - T$ plane that can be accessed by experiments. These can guide us in our search for the CP as well as the hadron-quark phase transition line. Their detection will also signal unambiguously the creation of a novel phase of QCD matter unlike the HRG phase. However, we should caution the reader that unlike critical exponents, sign structures of cumulants and the region over which they are negative are model dependent. Thus, our results should be viewed with caution when we want to extrapolate to real QCD. Another caveat is that , currently this study is at the mean field level. As an immediate step, the fate of these negative structures on including beyond mean field physics needs to be worked out. We also hope that our work motivates a similar study on the LQCD front on the sign structures of the off-diagonal susceptibilities which have so far been ignored.

IV. ACKNOWLEDGEMENTS

SC acknowledges “Centre for Nuclear Theory” [PIC XII-R&D-VEC-5.02.0500], Variable Energy Cyclotron Centre for support. KAM acknowledges the support by the National Science Foundation under Grant No. PHY-0854889. The authors would like to thank the organizers of WHEPP-2013 (Workshop on High Energy Particle Physics and Phenomenology) where part of this work was done. KAM would like to thank K. Sridhar and the Department of Theoretical Physics, TIFR (Mumbai) for hospitality where part of this work was done.

---

[1] L. D. McLerran and B. Svetitsky, Phys.Rev. **D24**, 450 (1981).
[2] B. Svetitsky, Phys.Rept. **132**, 1 (1986).
[3] Y. Aoki, G. Endrodi, Z. Fodor, S. Katz, and K. Szabo, Nature **443**, 675 (2006), arXiv:hep-lat/0611014 [hep-lat].
[4] C. Schmidt (HotQCD Collaboration), AIP Conf.Proc. **1343**, 513 (2011), arXiv:1012.2230 [hep-lat].
[5] S. Borsanyi, G. Endrodi, Z. Fodor, S. Katz, S. Krieg, et al., JHEP **1208**, 053 (2012), arXiv:1204.6710 [hep-lat].

[6] O. Kaczmarek, F. Karsch, E. Laermann, C. Miao, S. Mukherjee, et al., Phys.Rev. **D83**, 014504 (2011), arXiv:1011.3130 [hep-lat].
[7] P. de Forcrand, PoS **LAT2009**, 010 (2009), arXiv:1005.0539 [hep-lat].
[8] S. Gupta, PoS **LATTICE2010**, 007 (2010), arXiv:1101.0109 [hep-lat].
[9] P. N. Meisinger and M. C. Ogilvie, Phys.Lett. **B379**, 163 (1996), arXiv:hep-lat/9512011 [hep-lat].
[10] K. Fukushima, Phys.Lett. **B591**, 277 (2004), arXiv:hep-ph/0310121 [hep-ph].
[11] C. Ratti, M. A. Thaler, and W. Weise, Phys.Rev. **D73**, 014019 (2006), arXiv:hep-ph/0506234 [hep-ph].
[12] S. K. Ghosh, T. K. Mukherjee, M. G. Mustafa, and R. Ray, Phys.Rev. **D73**, 114007 (2006), arXiv:hep-ph/0603050 [hep-ph].
[13] B.-J. Schaefer, J. M. Pawlowski, and J. Wambach, Phys.Rev. **D76**, 074023 (2007), arXiv:0704.3234 [hep-ph].
[14] H. Mao, J. Jin, and M. Huang, J.Phys. **G37**, 035001 (2010), arXiv:0906.1324 [hep-ph].
[15] B.-J. Schaefer and M. Wagner, Phys.Rev. **D79**, 014018 (2009), arXiv:0808.1491 [hep-ph].
[16] J. T. Lenaghan, D. H. Rischke, and J. Schaffner-Bielich, Phys.Rev. **D62**, 085008 (2000), arXiv:nucl-th/0004006 [nucl-th].
[17] K. Fukushima and T. Hatsuda, Rept.Prog.Phys. **74**, 014001 (2011), arXiv:1005.4814 [hep-ph].
[18] R. Ray, Nucl.Phys. **A862-863**, 118 (2011).
[19] B. Mohanty, (2013), arXiv:1311.3722 [nucl-ex].
[20] M. A. Stephanov, K. Rajagopal, and E. V. Shuryak, Phys.Rev.Lett. **81**, 4816 (1998), arXiv:hep-ph/9806219 [hep-ph].
[21] M. A. Stephanov, K. Rajagopal, and E. V. Shuryak, Phys.Rev. **D60**, 114028 (1999), arXiv:hep-ph/9903292 [hep-ph].
[22] V. Koch, A. Majumder, and J. Randrup, Phys.Rev.Lett. **95**, 182301 (2005), arXiv:nucl-th/0505052 [nucl-th].
[23] C. Bernard et al. (MILC Collaboration), Phys.Rev. **D71**, 034504 (2005), arXiv:hep-lat/0405029 [hep-lat].
[24] C. Bernard, C. E. DeTar, L. Levkova, S. Gottlieb, U. Heller, et al., Phys.Rev. **D77**, 014503 (2008), arXiv:0710.1330 [hep-lat].
[25] M. Cheng, P. Hendge, C. Jung, F. Karsch, O. Kaczmarek, et al., Phys.Rev. **D79**, 074505 (2009), arXiv:0811.1006 [hep-lat].
[26] S. Borsanyi, Z. Fodor, S. D. Katz, S. Krieg, C. Ratti, et al., JHEP **1201**, 138 (2012), arXiv:1112.4416 [hep-lat].
[27] K. Fukushima, Phys.Rev. **D77**, 114028 (2008), arXiv:0803.3318 [hep-ph].
[28] W.-j. Fu, Y.-x. Liu, and Y.-L. Wu, Phys.Rev. **D81**, 014028 (2010), arXiv:0910.5783 [hep-ph].
[29] W.-j. Fu and Y.-l. Wu, Phys.Rev. **D82**, 074013 (2010), arXiv:1008.3684 [hep-ph].
[30] A. Bhattacharyya, P. Deb, A. Lahiri, and R. Ray, Phys.Rev. **D82**, 114028 (2010), arXiv:1008.0768 [hep-ph].
[31] A. Bhattacharyya, P. Deb, A. Lahiri, and R. Ray, Phys.Rev. **D83**, 014011 (2011), arXiv:1010.2394 [hep-ph].
[32] B.-J. Schaefer, M. Wagner, and J. Wambach, Phys.Rev. **D81**, 074013 (2010), arXiv:0910.5628 [hep-ph].
[33] J. Wambach, B.-J. Schaefer, and M. Wagner, Acta Phys.Polon.Supp. **3**, 691 (2010), arXiv:0911.0296 [hep-ph].
[34] S. Gupta, Pramana **76**, 801 (2011).
[35] A. Bazavov, H. Ding, P. Hegde, O. Kaczmarek, F. Karsch, et al., Phys.Rev.Lett. **109**, 192302 (2012), arXiv:1208.1220 [hep-lat].
[36] S. Borsanyi, Z. Fodor, S. Katz, S. Krieg, C. Ratti, et al., Phys.Rev.Lett. **111**, 062005 (2013), arXiv:1305.5161 [hep-lat].
[37] B. Schaefer and M. Wagner, Phys.Rev. **D85**, 034027 (2012), arXiv:1111.6871 [hep-ph].
[38] B. Berdnikov and K. Rajagopal, Phys.Rev. **D61**, 105017 (2000), arXiv:hep-ph/9912274 [hep-ph].
[39] C. Nonaka and M. Asakawa, Phys.Rev. **C71**, 044904 (2005), arXiv:nucl-th/0410078 [nucl-th].
[40] M. Asakawa, S. Ejiri, and M. Kitazawa, Phys.Rev.Lett. **103**, 262301 (2009), arXiv:0904.2089 [nucl-th].
[41] V. Skokov, B. Friman, F. Karsch, and K. Redlich, J.Phys. **G38**, 124102 (2011), arXiv:1108.1300 [hep-ph].
[42] B. Friman, F. Karsch, K. Redlich, and V. Skokov, Eur.Phys.J. **C71**, 1694 (2011), arXiv:1103.3511 [hep-ph].
[43] R. Gavai and S. Gupta, Phys.Lett. **B696**, 459 (2011), arXiv:1001.3796 [hep-lat].
[44] L. Adamczyk et al. (STAR Collaboration), (2013), arXiv:1309.5681 [nucl-ex].
[45] S. Chatterjee and K. A. Mohan, Phys.Rev. **D85**, 074018 (2012), arXiv:1108.2941 [hep-ph].
[46] S. Chatterjee and K. A. Mohan, Phys.Rev. **D86**, 114021 (2012), arXiv:1201.3352 [hep-ph].
[47] A. Walther and A. Griewank, in Combinatorial Scientific Computing, edited by U. Naumann and O. Schenk (Chapman-Hall CRC Computational Science, 2012) Chap. 7, pp. 181–202.
[48] M. Wagner, A. Walther, and B.-J. Schaefer, Comput.Phys.Commun. **181**, 756 (2010), arXiv:0912.2208 [hep-ph].
[49] A. Bazavov, H. T. Ding, P. Hegde, O. Kaczmarek, F. Karsch, et al., (2014), arXiv:1404.6511 [hep-lat].
[50] J. Cleymans and K. Redlich, Phys.Rev.Lett. **81**, 5284 (1998), arXiv:nucl-th/9808030 [nucl-th].
[51] A. Andronic, P. Braun-Munzinger, and J. Stachel, Nucl.Phys. **A772**, 167 (2006), arXiv:nucl-th/0511071 [nucl-th].
[52] F. Becattini, J. Manninen, and M. Gazdzicki, Phys.Rev. **C73**, 044905 (2006), arXiv:hep-ph/0511092 [hep-ph].
[53] S. Chatterjee, R. Godbole, and S. Gupta, Physics Letters B **727**, 554 (2013), arXiv:1306.2006 [nucl-th].